Diameter-selective near-field Raman analysis and imaging of isolated carbon nanotube bundles

Taka-aki Yano, Prabhat Verma, and Satoshi Kawata[a)]
Department of Applied Physics, Osaka University, Suita, Osaka 565-0871, Japan

Yasushi Inouye[a),b)]
Graduate School of Frontier Biosciences, Osaka University, Suita, Osaka 565-0871, Japan

(Received 30 September 2005; accepted 14 January 2006; published online 3 March 2006)

Tip-enhanced near-field Raman scattering has been utilized to demonstrate the measurement of the distribution of single-walled carbon nanotubes (SWNTs) with a spatial resolution far beyond the diffraction limit of the probing light. This was done by measuring the radial breathing mode (RBM) of SWNTs in the near-field Raman spectra, which corresponded to the diameters of various SWNTs in the immediate vicinity of the tip. Further, near-field Raman imaging of the RBM provided a super-resolved color mapping corresponding to the diameter distribution of SWNTs within a bundle, which is not possible to realize by conventional topographic imaging methods. © *2006 American Institute of Physics*. [DOI: 10.1063/1.2178490]

Raman spectroscopy has been a promising tool to analyze single-walled carbon nanotubes (SWNTs).[1,2] The radial breathing mode (RBM), which appears in the low-frequency region (100–400 cm^{-1}) in a Raman spectrum, is one of the most significant vibrational modes of SWNTs, because this mode has much stronger dependency on the diameter of the SWNTs than the other vibrational modes.[2,3] From the position of the RBM in a Raman spectrum, the diameter of SWNTs can be determined with an accuracy of an angstrom. However, due to the diffraction limit of light, conventional micro-Raman spectroscopy provides an averaged detection of Raman scattering from SWNTs lying inside the illumination focal spot,[4] and hence the information about diameter distribution within the diffraction-limited focal area is lost. In order to overcome this diffraction limit, tip-enhanced near-field Raman spectroscopy (TERS),[5–7] which is based on the field enhancement at an apertureless metallic tip apex due to the localized surface plasmon polariton (LSPP) excitation,[8–10] has been utilized. With this powerful method, individual isolated SWNTs were measured and characterized by some of the present authors,[11] and also by others.[12]

In this letter, we demonstrate a measurement of the distribution of SWNTs with various diameters in a bundle using TERS. The possibility of resonant Raman effect in the SWNTs during the TERS experiments was also considered, and it was observed that the field enhancement under the nonresonant condition was also significant. By means of achieving a high-resolution monochromatic near-field Raman image of the SWNT bundles, it was shown that the isolated individual bundles can be imaged with a spatial resolution far beyond the diffraction limit of the probing light. Further, in order to map the diameter distribution within an individual bundle, a color-coded super-resolved tip-enhanced near-field Raman imaging of the bundle was carried out.

The SWNTs examined in the present study were produced using the high-pressure CO technique by the Carbon Nanotechnologies Inc. (CNI). Individual bundles of SWNTs were exfoliated from the aggregates by means of ultrasonication. The experimental setup was especially designed and established for nano-Raman spectroscopy.[5,11,13] A 35 nm silver-coated AFM cantilever operated in contact mode was employed as the apertureless metallic tip, and a frequency-doubled $Nd:YVO_4$ laser ($\lambda = 532$ nm) was utilized as the probe light.

Figure 1(a) shows an atomic force microscope (AFM) image of an individual SWNT bundle obtained with a silver-coated tip. Figure 1(b) shows a line profile corresponding to the dashed line in Fig. 1(a). The tip-enhanced near-field Raman spectrum was measured by positioning the silver-coated tip at the location indicated by (i) in the image. As shown by the upper spectrum in Fig. 1(c), six peaks were clearly observed in the frequency region of RBM, which correspond to

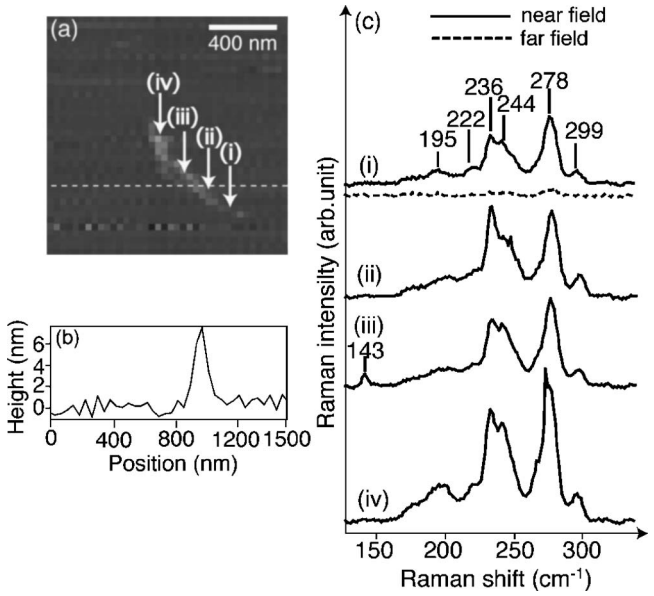

FIG. 1. (a) An AFM image of an individual SWNT bundle on the glass coverslip. (b) The line profile corresponding to the dashed line in the AFM image. (c) Tip-enhanced near-field Raman spectra measured over the bundle at the location indicated by (i)–(iv) in the AFM image.

[a)]Also at: RIKEN, Wako, Saitama 351-0198, Japan, and CREST, Japan Corporation of Science and Technology (JST), Kawaguchi 322-0012, Japan.
[b)]Electronic mail: ya-inoue@ap.eng.osaka-u.ac.jp

the SWNTs with different diameters, present in the bundle. SWNTs in a bundle exhibit 5%–10% higher RBM frequencies than the isolated SWNTs due to bundle effect caused by van der Waals interactions between the SWNTs.[14,15] According to a diameter (d) dependence of the frequency ω of the RBM including the bundle effect, i.e., $d\,[\mathrm{nm}]=232/(\omega-6.5)\,[\mathrm{cm}^{-1}]$,[15] the peaks in Fig. 1(c) at 195, 222, 236, 244, 278, and 299 cm^{-1} correspond to SWNTs of diameters 1.23, 1.07, 1.01, 0.97, 0.85 and 0.79 nm, respectively. When the metallic tip was moved away by 100 μm from the bundle (far field), the Raman scattering signal from the bundle became too weak to be analyzed, as can be seen by the dashed spectrum in Fig. 1(c). Only a trace of the strongest peaks could be observed in the far-field spectrum.

Assuming that the diameter of the enhanced light field, which is the same as the diameter of the tip apex, is 35 nm, and that the diameter of the focal spot, determined from the wavelength and the optics used, is 460 nm, the enhancement factor of the Raman scattering intensity for the radial breathing mode at 278 cm^{-1} was estimated to be about 200. On the other hand, the enhancement factor for Raman band at 236 cm^{-1} was estimated to be more than 1770, with the assumption that the intensity of far-field Raman scattering obtained without the tip is at most the standard deviation of the spectrum around the peak, because this peak was too weak to be distinguished from the background in the far-field spectrum. In the calculation of the enhancement factor, it was noted that the far-field component in the Raman signal comes from the whole bundle under the focal spot, while the near-field component originates only from the SWNTs present in the close vicinity of the tip apex.

The tip-enhanced near-field Raman spectra were measured, by scanning the sample stage along the bundle, at different locations indicated by (ii)–(iv) in the AFM image, and the corresponding spectra are shown by (ii)–(iv), respectively, in Fig. 1(c). While the far-field spectra remain identical for all locations, the near-field spectra shown in Fig. 1(c) differ from one another. For example, the near-field spectra (i) and (ii) show different intensity ratios between the peaks at 236 and 278 cm^{-1}, or the spectrum (iii) shows a peak at 143 cm^{-1}, which was not observed in other near-field spectra, indicating different diameter distributions at these three locations. The spectrum (iv) shows larger Raman intensities, suggesting that the density of the SWNTs is highest at that point.

With a closer analysis of the enhancement, it was found that the enhancement of Raman scattering, in most cases, was a combination of the enhancement due to the resonant Raman effect[1] and due to the LSPP excitation near the tip apex. The Kataura plot[3] shows that the third lowest transition energy (E_{33}^S) of semiconducting SWNTs and the second lowest transition energy (E_{22}^M) of metallic SWNTs with diameters between $\sim$0.8 to $\sim$1.5 nm are close to the incident photon energy (2.33 eV) used in the present experiments. Hence, the detected SWNTs with diameters between 0.79 and 1.23 nm experienced the resonant Raman effect. The net enhancement in the Raman scattering was therefore a combination of the resonant Raman effect and the near-field effect. In fact, it is well known that it is very difficult to observe SWNTs under nonresonant conditions.

The RBM band at 143 cm^{-1} in the near-field Raman spectrum at position (iii) in Fig. 1(c) corresponds to the SWNTs with a diameter of 1.70 nm. The Kataura plot shows

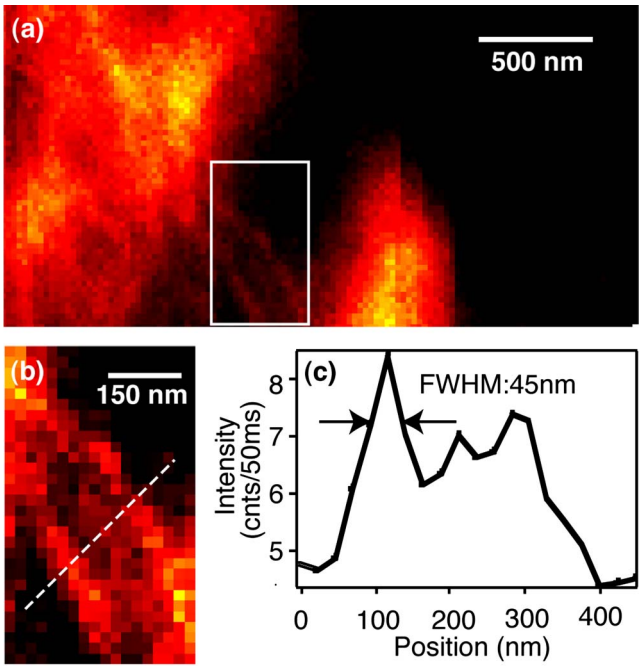

FIG. 2. (Color online) (a) Tip-enhanced near-field Raman image of SWNT bundles obtained at the frequency of 278 cm^{-1}. (b) A zoomed view of a part of the near-field Raman image which is surrounded by the square in (a). (c) The Raman intensity line-profile depicted by the dashed line in (b).

that the fourth lowest transition energy (E_{44}^S) of semiconducting SWNTs with a diameter of 1.70 nm is equal to the present excitation photon energy. However, since the optical absorption spectrum of E_{44}^S shows much weaker absorption than that of the lower transition energies (E_{11}^S, E_{22}^S, and E_{33}^S),[3] the resonant Raman effect can be neglected for this case. Therefore, it can be concluded that the enhancement for the mode at 143 cm^{-1} is associated only with the near-field effects. This result shows the possibility to detect nonresonant SWNTs without tuning the excitation wavelength to the resonant condition. The mechanical pressure applied to the SWNTs by the AFM-controlled tip, and the near-field effect as well as the tube-tube interaction can modify the bundle effect at each position of the probe. However, at this moment, the issue is still under investigation.

A spatial resolution far beyond the diffraction limit of the probing light was demonstrated by measuring a monochromatic near-field Raman image of SWNT bundles. The observation wave number in the spectrometer was set to 278 cm^{-1}, which corresponded to the RBM of SWNTs with a diameter of 0.85 nm, and the sample was scanned to obtain a near-field Raman image, shown in Fig. 2(a). The exit slit width of the spectrometer was adjusted to 140 μm, which corresponded to a spectral width of 0.2 nm (7 cm^{-1} at 539.9 nm). Considering the peak position and the peak width, this configuration is suitable for the peak at 278 cm^{-1} to pass through the slit completely.

Figure 2(b) is a zoomed view of the region surrounded by the square in Fig. 2(a), which shows the existence of two to three bundle structures in that region. Figure 2(c) shows the Raman intensity line-profile corresponding to the dashed line in Fig. 2(b). Judging from the full width at half-maxima of the first peak in the Raman line-profile, the diameter of the observed bundle is 45 nm, a value that is much smaller than the diffraction limit of the incident light. While the individual bundles are clearly observed in Fig. 2(b), multiple

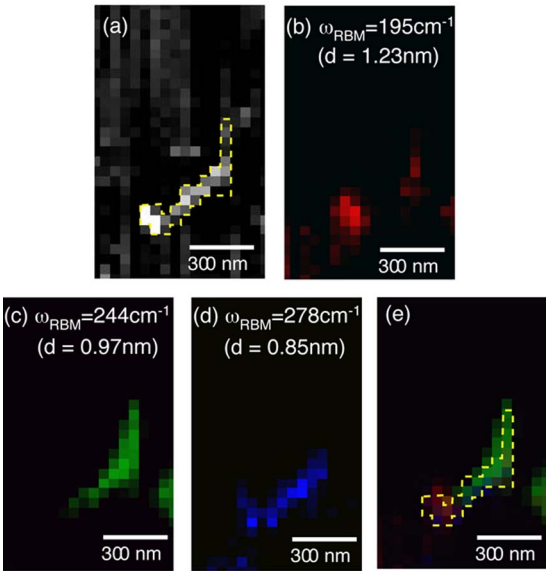

FIG. 3. (Color online) (a) An AFM image of a SWNT bundle. Tip-enhanced near-field Raman images were obtained at the frequencies (colors) of (b) 195 cm^{-1}, (c) 244 cm^{-1}, and (d) 278 cm^{-1}. (e) The mixed color image obtained by combining the three images in (b), (c), and (d).

bundle structures are not distinguishable in the other regions of Fig. 2(a). This is because the other regions have a high concentration of bundles, and hence the far-field background signal overwhelms the near-field Raman signal. The near-field signal is generated from only a few SWNTs in the close vicinity of the tip apex, while the far-field background originates from all the SWNTs present in the diffraction-limited focal spot, resulting in the reduction of the near-field to far-field signal ratio. Nevertheless, the monochromatic near-field Raman image in Fig. 2 clearly shows that the isolated individual SWNT bundles can be imaged with a high spatial resolution beyond the diffraction limits of the light.

Further, in order to identify the diameter distribution within a bundle, a diameter-selective near-field Raman imaging of an isolated SWNT bundle, using three different frequencies of RBM pre-selected from a tip-enhanced near-field Raman spectrum of the bundle, was performed. The area surrounded by the dotted line in Fig. 3(a), which is a topographic image of the sample, indicates the bundle selected for this study. The spectrometer was fixed at frequencies 195 cm^{-1} (diameter: 1.23 nm), 244 cm^{-1} (diameter: 0.97 nm) and 278 cm^{-1} (diameter: 0.85 nm), and the TERS images were obtained, which are shown in Figs. 3(b)–3(d), respectively. Figure 3(b) reveals that the SWNTs having a diameter of 1.23 nm are localized at both edges of the bundle, Fig. 3(b) shows that the SWNTs with a diameter of 0.97 nm are prominently distributed towards the central and upper part of the bundle, and Fig. 3(d) indicates that the SWNTs with a diameter of 0.85 nm are distributed mainly towards the lower part of the bundle. Figure 3(e) is a combination of the Figs. 3(b)–3(d), which compares well with the topographic image shown in Fig. 3(a). Apart from an image of the whole bundle, Fig. 3(e) also shows color-coded diameter distribution of the SWNTs within the bundle, which makes Fig. 3(e) much more informative than Fig. 3(a). This kind of imaging is not possible by conventional topographic imaging methods.

In conclusion, this study demonstrated a measurement of the distribution of SWNTs with diameters much smaller than the diffraction limit of the probing light, by utilizing the RBM in the tip-enhanced Raman spectra of the SWNTs bundles. A possibility of imaging isolated individual SWNT bundles with a spatial resolution beyond the diffraction limit of the probing light was shown. A super-resolved color-coded near-field Raman imaging of the diameter distribution of SWNTs within a bundle was also obtained, which revealed much more information about the bundle than the conventional topographic imaging methods.

One of the authors (Y.I.) gratefully acknowledges financial support by a Grant-in-Aid for Scientific Research Nos. 16360034 and 17034034 from the Ministry of Education, Culture, Sports, Science and Technology.

[1] A. M. Rao, E. Richter, S. Bandow, B. Chase, P. C. Eklund, K. A. Williams, S. Fang, K. R. Subbaswamy, M. Menon, A. Thess, R. E. Smalley, G. Dresselhaus, and M. S. Dresselhaus, Science **275**, 187 (1997).
[2] A. Jorio, R. Saito, J. H. Hafner, C. M. Lieber, M. Hunter, T. McClure, G. Dresselhaus, and M. S. Dresselhaus, Phys. Rev. Lett. **86**, 1118 (2001).
[3] H. Kataura, Y. Kumazawa, Y. Maniwa, I. Umezu, S. Suzuki, Y. Ohtsuka, and Y. Achiba, Synth. Met. **103**, 2555 (1999).
[4] C. Jiang, J. Zhao, H. A. Therese, M. Friedrich, and A. Mews, J. Phys. Chem. B **107**, 8742 (2003).
[5] Y. Inouye, N. Hayazawa, K. Hayashi, Z. Sekkat, and S. Kawata, Proc. SPIE **3791**, 40 (1999).
[6] M. Stockle, Y. D. Suh, V. Deckert, and R. Zenobi, Chem. Phys. Lett. **318**, 131 (2000).
[7] M. S. Anderson, Appl. Phys. Lett. **76**, 3130 (2000).
[8] Y. Inouye and S. Kawata, Opt. Lett. **19**, 159 (1994).
[9] U. C. Fischer and D. W. Pohl, Phys. Rev. Lett. **62**, 458 (1989).
[10] R. Bachelot, P. Gleyzes, and A. C. Boccara, Opt. Lett. **20**, 1924 (1995).
[11] N. Hayazawa, T. Yano, H. Watanabe, Y. Inouye, and S. Kawata, Chem. Phys. Lett. **376**, 174 (2003).
[12] A. Hartschuh, E. J. Sanchez, X. S. Xie, and L. Novotny, Phys. Rev. Lett. **90**, 95503 (2003).
[13] T. Ichimura, N. Hayazawa, M. Hashimoto, Y. Inouye, and M. S. Dresselhaus, Phys. Rev. Lett. **92**, 220801 (2004).
[14] L. Henrard, E. Hernandez, P. Bernier, and A. Rubio, Phys. Rev. B **60**, R8521 (1999).
[15] L. Alvarez, A. Righi, T. Guillard, S. Rols, E. Anglaret, D. Laplaze, and J. L. Sauvajol, Chem. Phys. Lett. **316**, 186 (2000).